

激光功率对 27SiMn 钢激光熔覆力学性能的影响

衡钊¹, 舒林森^{1,2*}¹陕西理工大学机械工程学院, 陕西 汉中 723001;²陕西省工业自动化重点实验室, 陕西 汉中 723001

摘要 为了获知激光功率对激光熔覆修复立柱用钢的影响规律,并找出熔覆层力学性能最优时的激光功率参数,采用单因素变量法,保持扫描速度 20 mm/s、送粉量 18 g/min、离焦量 0 和光斑直径 2 mm 不变,分别研究了激光功率为 1500,1800,2100,2400 W 时熔覆层的显微组织、拉伸性能及其断口形貌。结果表明:当激光功率为 1800 W 时,在立柱用钢表面上制备的 FeCrNiSi 合金涂层的热影响区深度最小值约为 360 μm ;涂层显微组织主体由均匀的胞状晶和柱状晶组成;涂层的延伸率在熔覆试件中最高,约为 5.3%;拉伸试件涂层断口呈韧性特征,涂层的塑性在熔覆试件中最强。综合考虑激光功率对 27SiMn 钢激光熔覆涂层的截面形貌、显微组织、力学行为特征以及断口形貌的影响,得出 1800 W 是最佳激光熔覆功率,在此功率下可制备出结合紧密且塑性较好熔覆涂层。

关键词 激光技术; 激光功率; 显微组织; 拉伸性能; 断口形貌

中图分类号 TG495

文献标志码 A

doi: 10.3788/CJL202249.0802011

1 引言

液压支架是现代煤矿综采的核心支护设备,而立柱是该设备的关键部件,其稳定性和可靠性是保证煤矿安全生产的关键^[1-3]。立柱长期服役在高应力、大湿度且含有硫、磷等腐蚀性介质的环境中,立柱用 27SiMn 钢材料表面常发生点蚀、磨损、鼓泡、剥落等^[4-5]失效问题,严重影响立柱强度及支护安全,故提高立柱用钢塑性是煤矿综采安全的保证。随着新环保要求的提高,用于液压支架立柱表面处理的电镀工艺已被淘汰。与之相比,激光熔覆技术利用激光能量将高性能合金材料快速熔凝,可在立柱用 27SiMn 钢表面形成基于冶金结合的高强、抗磨、防腐的功能涂层^[6-9]。激光熔覆工艺可对立柱失效特性进行绿色再制造复原^[10-12],技术优势突出,正逐步替代液压支架立柱零件的电镀工艺。

然而,激光熔覆成形机理非常复杂,若工艺参数

控制不当将影响制造质量,甚至产生微裂纹、气孔等缺陷^[13]。近年来,国内外学者对激光熔覆工艺进行了大量探究。蔡发等^[14]研究了立柱零件的激光熔覆修复工艺,制定了立柱激光熔覆修复的工艺流程并详细列出了工艺技术要求。宋勇等^[15]研究了奥氏体不锈钢熔覆层,发现氮含量对熔覆层的微观组织和力学性能有很大影响。Rashid 等^[16]研究了激光熔覆 300M 钢的力学性能及其断口形貌,发现沿横向路径熔覆的试样力学性能优于沿纵向、斜向 45°路径熔覆的试样。刘德来等^[17]研究了激光熔覆 Ni/316L 涂层的组织与力学性能,发现激光功率对熔覆组织、硬度和弹性模量有较大影响。杜学允等^[18]在 27SiMn 钢表面激光熔覆了不锈钢涂层,发现增加功率会降低涂层耐腐蚀性能。Teixeira 等^[19]在高锰钢表面激光熔覆了 1030A 合金,发现不同功率下涂层的显微组织以及耐磨性能有很大差异。

激光功率是影响熔覆涂层组织特征和力学性能

收稿日期: 2021-07-12; 修回日期: 2021-08-31; 录用日期: 2021-10-12

基金项目: 国家自然科学基金(51505268)、陕西省教育厅重点项目(20JS020)、陕西省教育厅专项科研项目(21JK0562)、陕西省工业自动化重点实验室开放课题研究基金(SLGPT2019KF01-16)、国防科技重点实验室基金(JCKY61420052022)

通信作者: *shulinsen19@163.com

的重要因素,但目前关于功率对 27SiMn 钢激光熔覆组织和力学行为特征影响的研究较少,尚缺乏系统讨论,不利于立柱零件激光熔覆再制造的工程应用。为了获知激光功率对激光熔覆修复立柱用钢的影响规律,设计了四种不同激光功率的多道单层激光熔覆工艺方案,利用超景深显微镜分析了不同功率下试样的截面形貌和显微组织特征,通过拉伸试验获得了不同功率下试样的应力-应变曲线,计算了其屈服强度、抗拉强度、延伸率、杨氏模量等力学性能指标,通过光学显微镜和扫描电镜(SEM)判定了熔覆涂层的断裂方式和塑性大小。研究结果为液压支架立柱零件的激光熔覆再制造修复提供了参考。

2 试 验

2.1 材 料

试验基体材料是液压支架立柱母材 27SiMn 钢,尺寸为 150 mm×80 mm×10 mm,其成分(质量分数,%)为:C(0.320),Si(1.250),Mn(1.200),P(0.030),S(0.032),Cu(0.300),Cr(0.300),Ni(0.300),Mo(0.150)。熔覆材料使用 FeCrNiSi 合金粉末,其成分(质量分数,%)为:C(0.75),Si(3.50),B(3.50),Cr(17.00),Ni(13.00),其余为 Fe 元素。该粉末外观形貌如图 1 所示,粉末颗粒球形成度较好,直径为 44~105 μm。

2.2 熔覆工艺及制样

熔覆试验由 3 kW 柔性光纤激光熔覆系统完成。该系统由 YLS3000 半导体激光器、ABB 六自由度机器人、ZF 环形熔覆头、CWFL 水冷装置和

RH-DFOM 双筒送粉装置组成,使用纯度(质量分数)为 99.9% 的氩气作为载粉气体和保护气体,采用“光内同轴”送粉模式,熔覆过程如图 2 所示。为了研究激光功率对力学性能的影响,通过工艺优化得到最优扫描速度、送粉量、离焦量、保护气流速度依次为 18 g/min、20 mm/s、0、10 L/min。采用的工艺参数如表 1 所示。

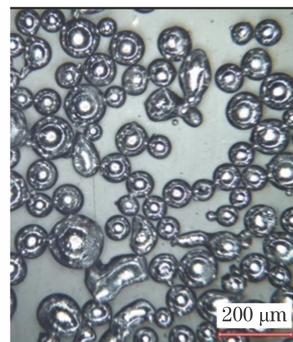


图 1 粉末形貌图

Fig. 1 Powder morphology

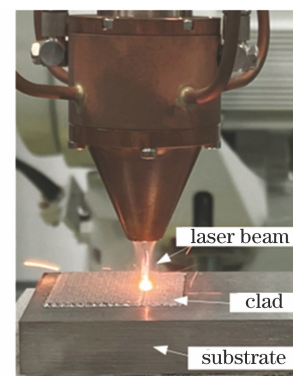


图 2 熔覆过程

Fig. 2 Melting and cladding process

表 1 熔覆工艺参数

Table 1 Melting and cladding process parameters

Sample No.	Laser power /W	Feeding rate / $(\text{g}\cdot\text{min}^{-1})$	Scanning speed / $(\text{mm}\cdot\text{s}^{-1})$	Defocusing amount /mm	Powder-sending flow / $(\text{L}\cdot\text{min}^{-1})$
S1	1500	18	20	0	10
S2	1800	18	20	0	10
S3	2100	18	20	0	10
S4	2400	18	20	0	10

图 3 是试样制备过程示意及试样尺寸示意图。首先,在 27SiMn 钢矩形板上预制尺寸(宽×深)为 15 mm×0.4 mm 的通槽,槽底设计为半径是 6 mm 的过渡圆角,如图 3(a)所示;然后,以 50% 的搭接率按纵向“弓”形路径熔覆,将烘干的 FeCrNiSi 合金粉末熔覆吹送到预制通槽中,高能束激光能量使之熔

化形成合金涂层;最后,利用线切割方法进行试件取样,拉伸试件(基材及 S1、S2、S3、S4)的取样位置和尺寸如图 3(c)、(d)所示,其中灰色区域为金相试件取样位置,其尺寸(长×宽×高)为 10 mm×7 mm×10 mm。

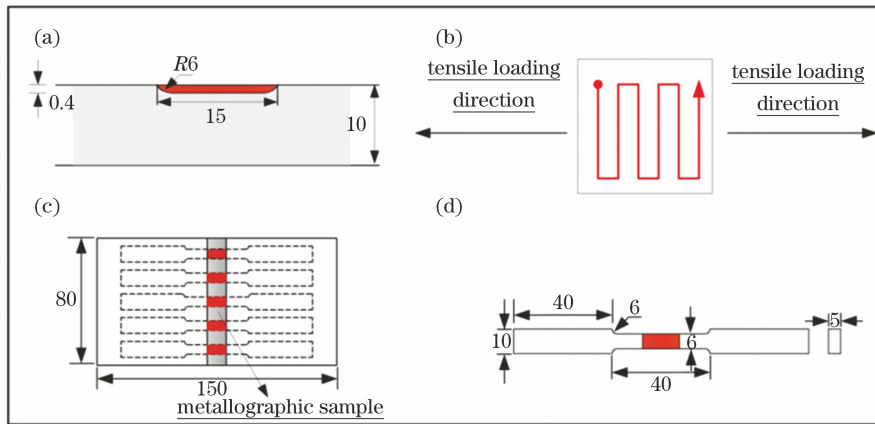


图 3 制样方案。(a)熔覆模型;(b)熔覆路径;(c)取样布局;(d)拉伸试样尺寸

Fig. 3 Sample making scheme. (a) Melting and cladding model; (b) melting and cladding path; (c) sampling layout; (d) specification of tensile specimen

2.3 测试与分析

第一步,采用砂纸对金相试件进行打磨、抛光,然后用质量分数为 4% 的硝酸乙醇溶液腐蚀 10 s,再通过 VHX-7000 型显微镜进行试件的金相观测,并对比分析 S1、S2、S3 和 S4 试样上熔覆层相同位置(上部、中部、下部)处的显微组织特征。

第二步,利用 WDW-100 复合材料试验机获取基材 27SiMn 钢和熔覆试样(S1~S4)的应力-应变曲线,设置拉伸应变速率为 0.001/s。试验中,试样动应变 ϵ 和动应力 σ 分别由视频引伸计和内置传感器采集。拉伸试件的力学性能指标为:

1)杨氏模量 E ,计算公式为 $E = \sigma / \epsilon$;

2)屈服强度 $\sigma_{0.2}$,其值为残余应变为 0.2% 时的应力值;

3)延伸率 δ ,其值为基材断裂时的最大应变值;

4)抗拉强度 σ_b ,取试件断裂前的最大应力。

第三步,通过 VHX-7000 型显微镜观察拉伸试件断口的整体宏观形貌,利用飞纳 Phenom™ 扫描电镜观察拉伸试件断口的微观形貌。

3 结果与讨论

3.1 熔覆层截面形貌及组织

图 4 为不同功率下获得的金相试件截面图。可以看出,熔覆层顶端都存在少量未熔化粉末颗粒,这

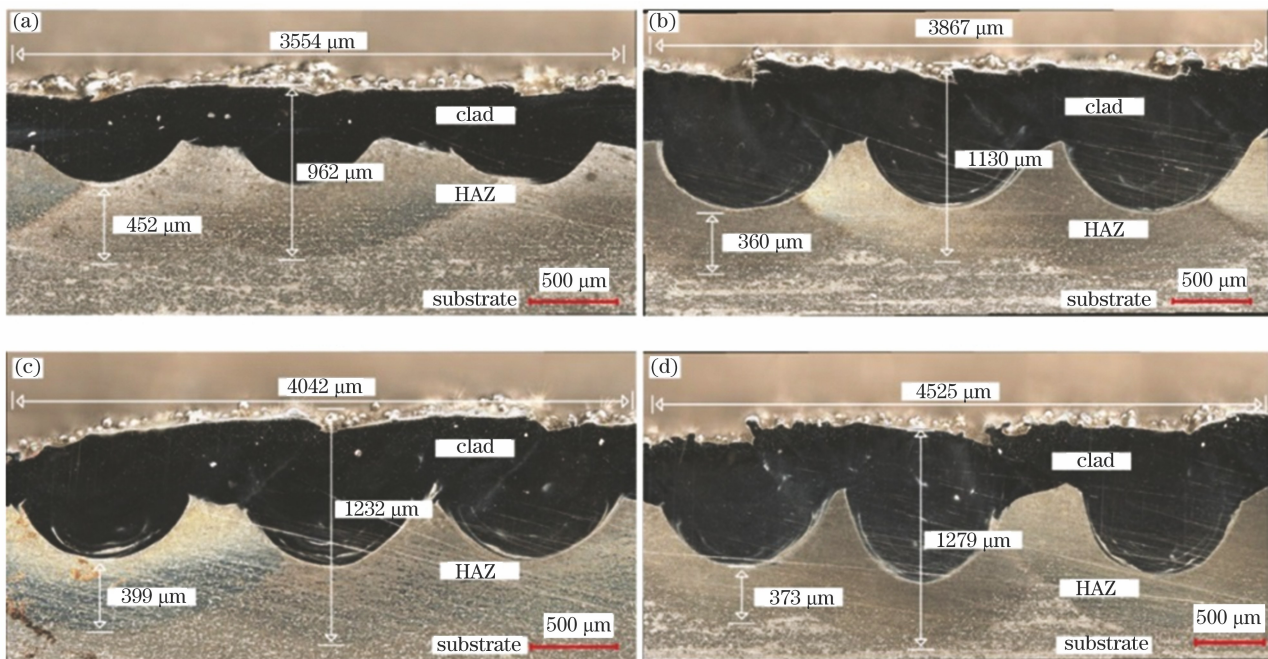


图 4 不同功率下的熔覆层截面。(a) 1500 W;(b) 1800 W;(c) 2100 W;(d) 2400 W

Fig. 4 Cross sections of cladding layer at different powers. (a) 1500 W; (b) 1800 W; (c) 2100 W; (d) 2400 W

是因为在激光熔覆过程中,输送的粉末没有被完全熔化,故粉末粘着在熔覆层表面。不同功率下的熔覆层特征极其相似,但是熔覆层总高度、熔覆层长度及热影响区(HAZ)深度存在差异。随着激光功率的增大,熔覆层顶端到热影响区最底端的总高度依次为 962,1130,1232,1279 μm ,呈现逐渐增大的趋势;熔覆层宽度依次为 3554,3867,4042,4525 μm ,增大趋势明显;热影响区深度依次为 452,360,399,373 μm ,呈现出先减小后增大的趋势。可知功率为 1800 W 时,热影响区深度呈现最小值 360 μm ,此时激光功率对基材的损伤程度最小。

图 5 为不同功率下熔覆试样的显微组织。激光熔覆是一个快热、快凝的过程,组织生长方向是从熔池底部向熔池顶部生长,其组织形态与温度梯度(G)、凝固速率(R)密切相关。图 5(a₃)~(d₃)所示为不同功率下的熔覆层下部组织。当激光功率相对

较低时,柱状晶数量少,晶粒尺寸小;随着激光功率的增大,熔覆层下部紧贴基材,散热较快,温度梯度 G 增大,凝固速率 R 减小,使得 G/R 值增大,晶体生长速度大于形核速度,故形成的柱状晶逐渐粗大。

图 5(a₂)~(d₂)所示为不同功率下的熔覆层中部组织。当激光功率为 1500 W 时,其组织主体形态由胞状晶和柱状晶以及少量的树枝晶组成;当激光功率增大到 1800 W 时,部分胞状晶生长为柱状晶和树枝晶,但是晶粒形态逐步趋向均匀;当继续增加激光功率时,温度梯度 G 增大, G/R 值增大,中部区域的晶体组织生长更充分,形成了晶粒尺寸较大的树枝晶。

图 5(a₁)~(d₁)所示为不同功率下的熔覆层上部组织。随着激光功率的增加, G/R 值增大,此时晶体生长速度大于形核速度,故形成的树枝晶和柱状晶的晶粒尺寸逐渐变大且树枝晶占比升高。

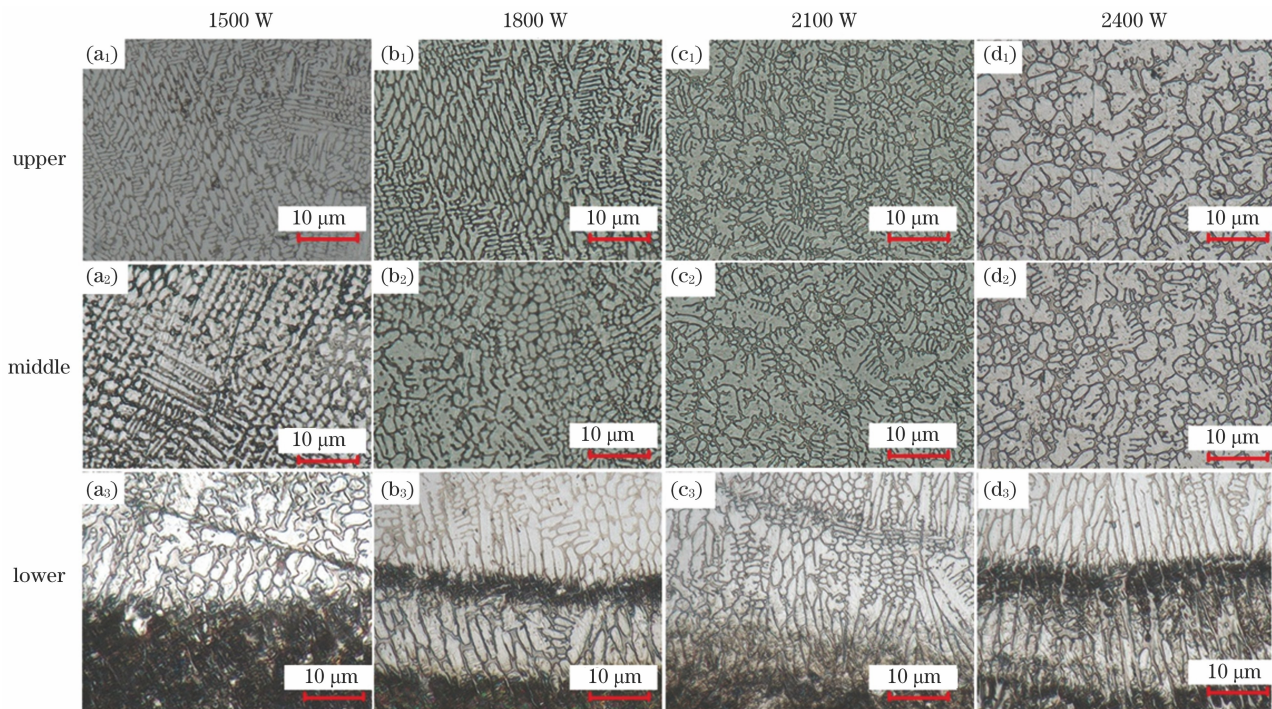


图 5 不同激光功率下熔覆层上部、中部和下部的显微组织

Fig. 5 Microstructures of upper, middle, and lower parts of cladding layer at different laser powers

3.2 熔覆层拉伸性能分析

图 6 为试件拉伸前后的形貌。可以看出,基材出现明显的颈缩,在试样中部断开,断口倾斜角度大,而四种熔覆试样的颈缩不显著,断口较为整齐,熔覆试件的力学性能低于基材。

五种试件的应力-应变曲线及力学指标对比分别如图 7、8 所示。与基材相比,S1 试件的屈服强度增强 1%,为 750 MPa,杨氏模量增高 32%,抗拉强度降低 17%,延伸率降低 92%,可知 1500 W 功率

下熔覆试件抵抗微量变形的能力很强,同时脆性又很高。而其余熔覆试件的力学性能均低于基材。S2 试件的延伸率为 5.3%,因其延伸率大于 5%,故呈现为塑性变形,其塑性变形能力在所有熔覆试件中最强,其屈服强度和杨氏模量分别为 655 MPa 和 130 GPa,具有较强抵抗变形的能力。S3 试件的屈服强度和延伸率分别为 716 MPa 和 1.5%,但其塑性变形能力太弱。S4 试件的四种力学性能指标都最低,力学性能最差。综合来看,按试件屈服强度及

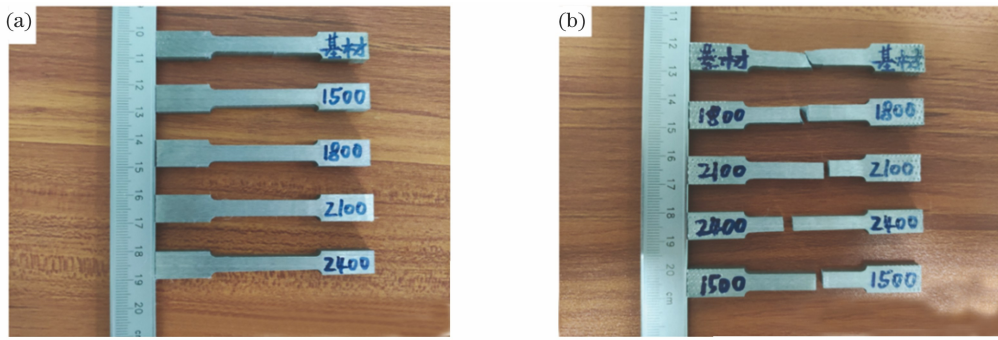


图 6 试件拉伸前后的形貌。(a)拉伸前;(b)拉伸后

Fig. 6 Morphologies before and after specimen stretching. (a) Before stretching; (b) after stretching

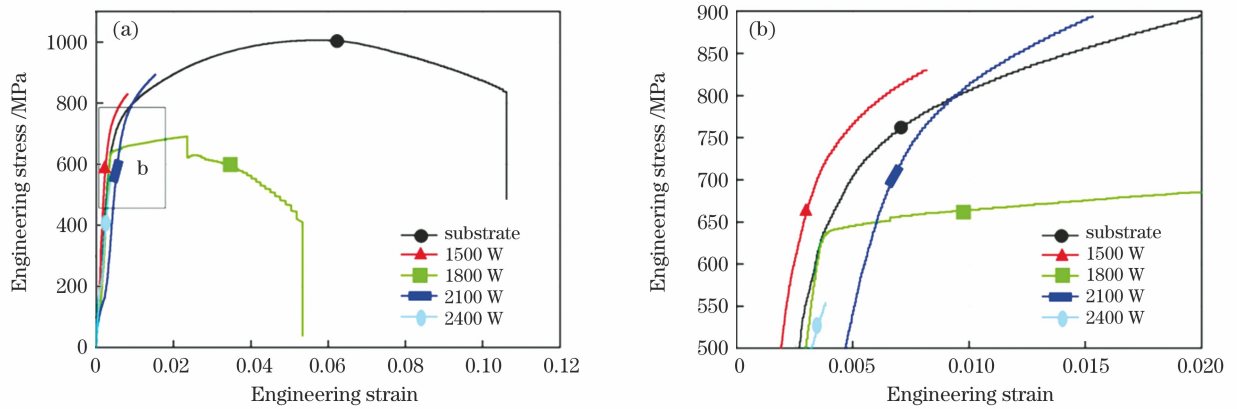


图 7 五种拉伸试件的应力-应变关系。(a)应力-应变曲线图;(b)局部放大图

Fig. 7 Stress-strain relationships for five types of tensile specimens. (a) Stress-strain curve; (b) local magnification

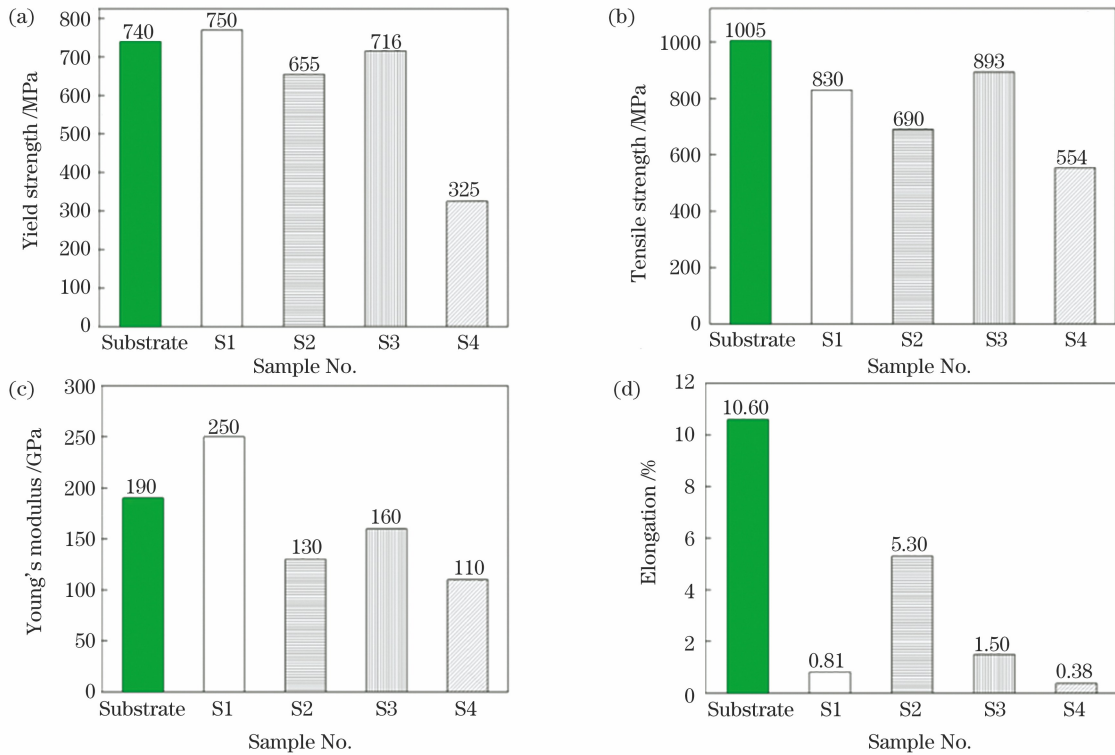


图 8 五种拉伸试件的力学性能对比。(a)屈服强度;(b)抗拉强度;(c)杨氏模量;(d)延伸率

Fig. 8 Mechanical property comparison among five tensile specimens. (a) Yield strength; (b) tensile strength; (c) Young's modulus; (d) elongation

延伸率的优良顺序,对应的激光功率依次为 1800 W、2100 W、1500 W、2400 W,可知,激光功率从 1500 W 增加到 1800 W 时,试件的塑性不断增高,从 1800 W 增加到 2400 W 时,试件的塑性持续降低。这是由于随着激光功率的增加,试件组织中的树枝晶、柱状晶增多,细长状的柱状晶和粗大的树枝晶易使试件发生断裂,导致其拉伸性能下降。尽管 1500 W 熔覆试件以胞状晶和柱状晶为主,但其中部区域存在少量大尺寸树枝晶和柱状晶,整体性能略低于 2100 W 试样。

3.3 拉伸断口分析

图 9 为 S1~S4 试件和基材的拉伸断口形貌。

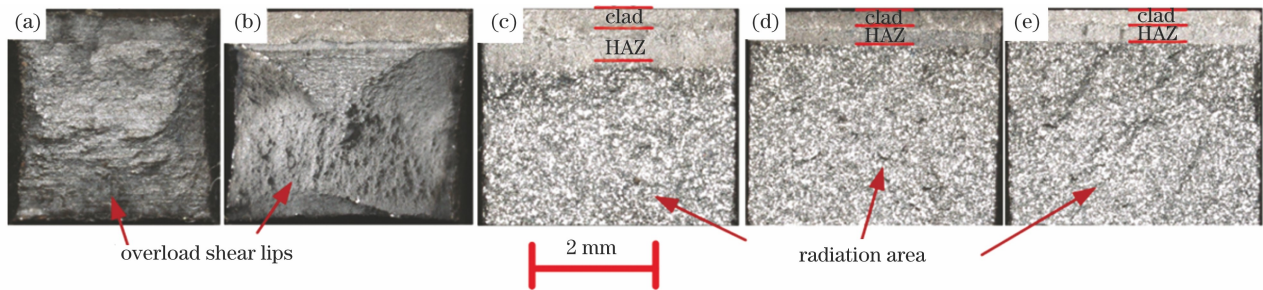


图 9 五种拉伸试件断口形貌。(a)基材;(b)S1;(c)S2;(d)S3;(e)S4

Fig. 9 Fracture morphologies of five kinds of tensile specimens. (a) Substrate; (b) S1; (c) S2; (d) S3; (e) S4

图 10 为 S1~S4 试件的断口形貌 SEM 图。图 10 (a₁)~(d₁)是熔覆层的断口形貌,可以看出,

其中,基材和 S1 发生大量塑性变形,延伸率超过 5% [图 8 (d)],故以韧性方式失效 (Ductile Failure),呈现出典型的尖锥形断口。与基材试样相比,S2 的剪切唇区域小于基材,可见其塑性低于基材。S1、S2、S3 断口平齐光亮,由许多发光的解理小刻面组成,且发生微量的塑性变形 [图 8 (d)],故以脆性方式失效 (Brittle Failure),形成典型的脆性解理断口。断口由三部分组成,分别为纤维区、放射区和剪切唇,由图 9 可知,纤维区由熔覆区和热影响区组成,放射区为基体,剪切唇区域极小。裂纹通常起于纤维区,向放射区延伸。

S1、S3、S4 断口平齐、光滑,熔覆层断裂属于脆性解理断裂,主要是由于 FeCrNiSi 合金粉末中的 C、Si

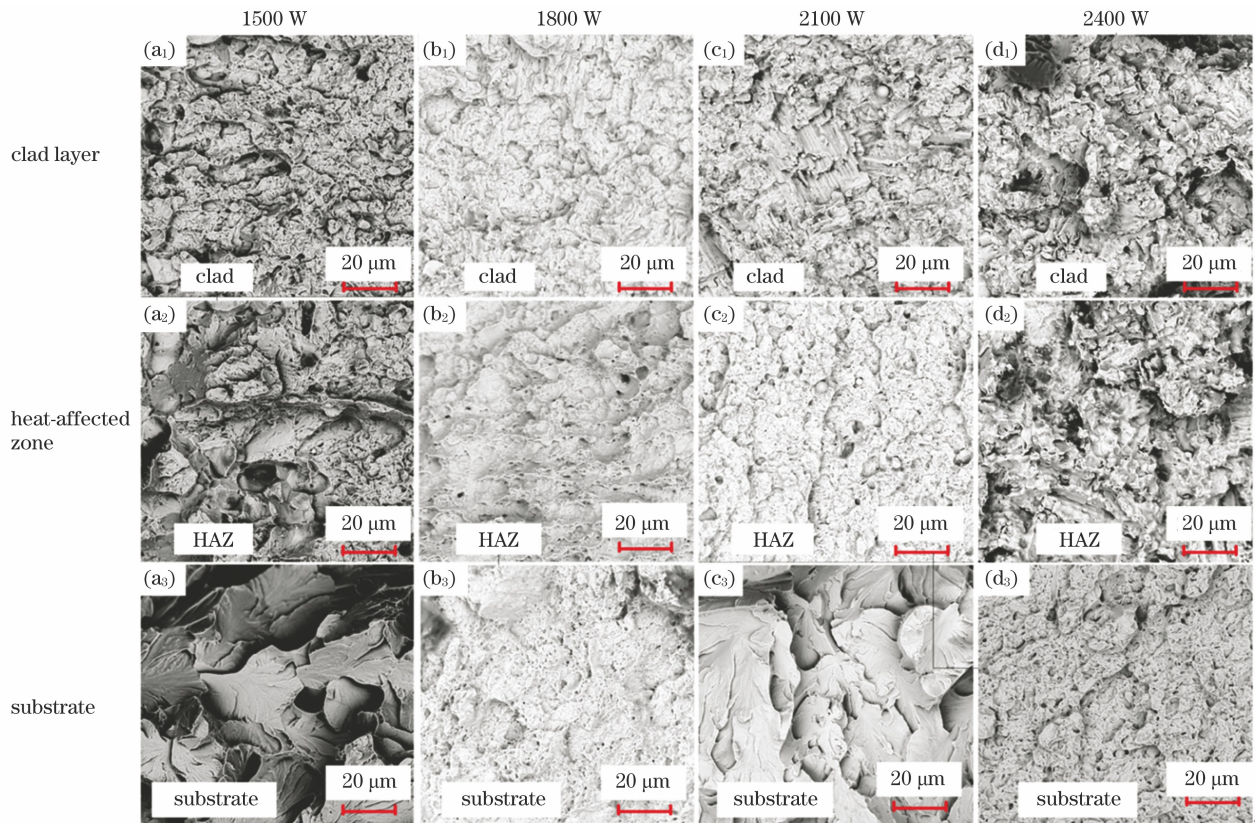


图 10 不同激光功率下熔覆层、热影响区和基体的断口形貌

Fig. 10 Fracture morphologies of cladding layers, heat-affected zones and substrates at different laser powers

元素含量较高,熔覆层脆性增高;S2 断口主体呈现脆性特征,但也存在少量微小韧窝,其断裂方式属于准解理断裂。图 10(a₂)~(d₂)是热影响区的断口形貌,S1、S4 断口光滑,组织中存在由解理面形成的解理台阶,断口呈现脆性特征;S2、S3 断口组织中存在较小韧窝,呈现出韧性特征。图 10(a₃)~(d₃)是基体的断口形貌,S1、S3 断口呈现出典型的河流花样特征,其断裂方式为典型的脆性解理断裂;S2、S4 断口也存在许多较小韧窝,这些韧窝通常都会长大且连接起来形成裂纹,造成微孔聚集型断裂。通过对比可以得出,S2 的熔覆层、热影响区和基体的断口都存在韧窝,呈现出韧性特征,塑性最高。而其余试件的熔覆层、热影响区或者基体,其中某一部分断口呈现出脆性特征,塑性弱于 S2。

4 结 论

探究了激光功率对 27SiMn 钢表面激光熔覆 FeCrNiSi 的影响,通过分析熔覆层的截面、显微组织、拉伸性能以及断口形貌,得到以下结论。

1)熔覆层宽度随激光功率的增加而增大,热影响区深度则随激光功率的增加呈先减小后增大的趋势。在熔覆层中部组织中,1800 W 试件的组织主要由胞状晶以及少量柱状晶、树枝晶组成,其组织形态趋于均匀;而其余功率试件的组织以细长的柱状晶和形态较大的树枝晶为主。

2)综合考察试件的屈服强度、抗拉强度、杨氏模量和延伸率,发现激光功率从 1500 W 增加到 1800 W 时,熔覆试件的塑性不断增高,激光功率从 1800 W 增加到 2400 W 时,其塑性持续降低。得到 1800 W 熔覆试件的力学性能最优,其屈服强度、抗拉强度、杨氏模量和延伸率依次为 655 MPa、690 MPa、130 GPa、5.3%,表现出了部分塑性变形的力学特性。

3)对比发现,1800 W 试样的熔覆层、热影响区和基体的断口都存在微小韧窝,表现出韧性断裂特征,而其余试件的熔覆层、热影响区和基体存在解理台阶或河流花样形脆性解理断裂特征。

参 考 文 献

- [1] Chai R X, Li K K, Guo W, et al. Effect of laser power on microstructure and properties of Fe-based alloy coating on surface of 27SiMn steel by laser cladding[J]. Heat Treatment of Metals, 2018, 43(8): 136-141.
柴蓉霞, 李凯凯, 郭卫, 等. 激光功率对 27SiMn 钢表面激光熔覆铁基合金组织和性能的影响[J]. 金属热处理, 2018, 43(8): 136-141.
- [2] Song P F, Jiang F L, Wang Y L, et al. Advances in the preparation of high entropy alloy coatings by laser cladding[J]. Surface Technology, 2021, 50(1): 242-252, 286.
宋鹏芳, 姜芙林, 王玉玲, 等. 激光熔覆制备高熵合金涂层研究进展[J]. 表面技术, 2021, 50(1): 242-252, 286.
- [3] Zhang D N, Fu H G, Xing Z G, et al. Effect and mechanism of CeO₂ on the microstructure and properties of Ni60A - Cr₃C₂ laser cladding layer[J]. Surface Review and Letters, 2021, 28(4): 2150018.
- [4] Pang X T, Yao C W, Gong Q F, et al. Influence of multilayer laser cladding on the microstructure and properties of 30CrMnSiNi2A steel substrate [J]. Chinese Journal of Lasers, 2021, 48(6): 0602104.
庞小通, 姚成武, 龚群甫, 等. 多层激光熔覆对 30CrMnSiNi2A 高强钢组织与性能的影响[J]. 中国激光, 2021, 48(6): 0602104.
- [5] Wang Z, Shang X J, Tian X Q, et al. Effects of laser cladding process parameters on microstructure and properties of MoFeCrTiWAlNb high-melting-point and high-entropy alloy coating [J]. Materials Protection, 2021, 54(4): 94-101, 112.
汪震, 尚晓娟, 田兴强, 等. 激光熔覆工艺参数对 MoFeCrTiWAlNb 高熔点高熵合金涂层组织和性能的影响[J]. 材料保护, 2021, 54(4): 94-101, 112.
- [6] Liu S T, Ban C Y, Zhang J W, et al. Study on the microstructure of Ni60 coatings by electromagnetic field assisted laser cladding[J]. Journal of Physics: Conference Series, 2021, 1865(2): 022058.
- [7] Wang Q, Li Y Y, Yang H B, et al. Effect of laser power on laser cladding structure and hardness of 17-4PH wire [J]. Surface Technology, 2021, 50(3): 191-197.
王强, 李洋洋, 杨洪波, 等. 激光功率对 17-4PH 丝材激光熔覆组织及硬度的影响[J]. 表面技术, 2021, 50(3): 191-197.
- [8] Huang L F, Sun Y N, Wang G J. Research progress of laser cladding high-entropy alloy coating[J]. Laser & Optoelectronics Progress, 2019, 56(24): 240003.
黄留飞, 孙耀宁, 王国建. 激光熔覆技术制备高熵合金涂层研究进展[J]. 激光与光电子学进展, 2019, 56(24): 240003.
- [9] Xu Y F, Sun Y N, Wang G J, et al. Microstructure and properties of iron-based alloys coatings prepared by high-speed laser cladding[J]. Chinese Journal of Lasers, 2021, 48(10): 1002122.
徐一飞, 孙耀宁, 王国建, 等. 高速激光熔覆铁基合金涂层的组织及性能研究[J]. 中国激光, 2021, 48

- (10): 1002122.
- [10] Ni X J, Zhang B W, Zhao Z X, et al. Investigation on the microstructure and properties of the laser cladded $\text{Mo}_2\text{NiB}_2 - \text{Cr}_7\text{C}_3$ composite coatings [J]. *Surface Technology*, 2021, 50(5): 60-69.
倪晓杰, 张博文, 赵忠贤, 等. 激光熔覆 $\text{Mo}_2\text{NiB}_2 - \text{Cr}_7\text{C}_3$ 复合陶瓷熔覆层组织结构与性能研究 [J]. *表面技术*, 2021, 50(5): 60-69.
- [11] Wang Y F, Zhao X Y, Lu W J, et al. Microstructure and properties of high speed laser cladding stainless steel coating on sucker rod coupling surfaces [J]. *Chinese Journal of Lasers*, 2021, 48(6): 0602114.
王彦芳, 赵晓宇, 陆文俊, 等. 抽油杆接箍表面高速激光熔覆不锈钢涂层的组织与性能 [J]. *中国激光*, 2021, 48(6): 0602114.
- [12] Li S C, Mo B, Xiao G, et al. Microstructure characteristics and their influence factors during laser additive manufacturing of metal materials [J]. *Laser & Optoelectronics Progress*, 2021, 58(1): 100007.
李时春, 莫彬, 肖罡, 等. 金属材料的激光增材制造微观组织结构特征及其影响因素 [J]. *激光与光电子学进展*, 2021, 58(1): 100007.
- [13] Shu L S, Wang J S, Bai H Q, et al. Numerical and experimental investigation on laser cladding treatment of wear shaft surface [J]. *Journal of Mechanical Engineering*, 2019, 55(9): 217-223.
舒林森, 王家胜, 白海清, 等. 磨损轴面激光熔覆过程的数值模拟及试验 [J]. *机械工程学报*, 2019, 55(9): 217-223.
- [14] Cai F, Liu H J. Analysis of laser cladding repairing technology of hydraulic support column [J]. *Mechanical Engineering & Automation*, 2016(4): 125-127, 129.
蔡发, 刘混举. 液压支架立柱激光熔覆技术修复工艺分析 [J]. *机械工程与自动化*, 2016(4): 125-127, 129.
- [15] Song Y, Zhu W, Li S, et al. Microstructure and properties of nitrogenous austenitic stainless steel prepared using laser cladding [J]. *Chinese Journal of Lasers*, 2020, 47(4): 0402004.
宋勇, 朱伟, 李胜, 等. 激光熔覆含氮奥氏体不锈钢层的组织与性能 [J]. *中国激光*, 2020, 47(4): 0402004.
- [16] Rashid R A R, Barr C J, Palanisamy S, et al. Effect of clad orientation on the mechanical properties of laser-clad repaired ultra-high strength 300M steel [J]. *Surface and Coatings Technology*, 2019, 380: 125090.
- [17] Liu D L, Wang B, Zhou P H, et al. Effect of laser power on microstructure and mechanical properties of high-speed laser clad Ni/316L layer [J]. *Heat Treatment of Metals*, 2021, 46(5): 213-218.
刘德来, 王博, 周攀虎, 等. 激光功率对高速激光熔覆 Ni/316L 层组织与力学性能的影响 [J]. *金属热处理*, 2021, 46(5): 213-218.
- [18] Du X Y, He J Q, Wang W, et al. Influence of laser power on corrosion resistance performance of cladding layer on 27SiMn stainless steel column [J]. *Mining & Processing Equipment*, 2018, 46(1): 59-64.
杜学芸, 何建群, 王伟, 等. 激光功率对 27SiMn 不锈钢立柱熔覆层耐蚀性能的影响 [J]. *矿山机械*, 2018, 46(1): 59-64.
- [19] Teixeira M F, Pacheco J T, Silva L J, et al. Wear resistance of a Metco 1030A hard coating deposited on Hadfield steel by laser cladding for ore comminution application [J]. *The International Journal of Advanced Manufacturing Technology*, 2021, 112(7/8): 1873-1884.

Effect of Laser Power on Mechanical Properties of Laser Cladded 27SiMn Steel

Heng Zhao¹, Shu Linsen^{1,2*}

¹ School of Mechanical Engineering, Shaanxi University of Technology, Hanzhong, Shaanxi 723001, China;

² Shaanxi Key Laboratory of Industrial Automation, Hanzhong, Shaanxi 723001, China

Abstract

Objective The laser cladding technology can generate a functional coating based on metallurgical combination of high strength, anti-wear, and corrosion resistance on the 27SiMn steel surface of hydraulic support column by rapidly melting and solidifying high performance alloy materials with laser energy, thus the strength and support safety performance of the column can be improved. However, during the coating generation process, a sub-stable material structure of multi-phase heterogeneous materials is formed inside the coating due to the complex thermo-physical

field reaction of the laser with the powder and the substrate. The laser parameters directly influence the microstructure and mechanical properties of the cladded coating, in which laser power is an important factor influencing the tissue characteristics and the mechanical properties of the cladded coating. However, there are few studies on the effect of laser power on the characteristics of the organization and the mechanical behaviors of laser cladded 27SiMn steels, which is not conducive to the engineering application of laser cladding and remanufacturing of column parts. In order to obtain the effect of laser power on the organization and properties of the 27SiMn steel repaired by laser cladding, and to find out the optimal laser power parameters for the cladding layer, the laser cladding process and the mechanical properties of the 27SiMn steel are studied experimentally.

Methods In this paper, the FeCrNiSi alloy powder is used as the material for preparing the coating. The alloy powder is blown onto the surface of the 27SiMn steel base material by a high-purity argon gas (mass fraction of 99.99%), while the alloy powder and the part of the metal on the surface of the base material are rapidly melted under the action of a high-energy laser beam to generate the alloy coating. First, a single-factor variable approach is used in the experiments. Four different laser cladding schemes with 1500 W, 1800 W, 2100 W, and 2400 W powers are designed to produce the specimens. The specimens are prepared on prefabricated straight slot with a overlapping ratio of 50% in a longitudinal “弓” path. Second, the cross-sectional morphologies and the microstructural characteristics of the specimens at four different powers are observed using the VHX-7000 ultra-deep field microscope, and the microstructural characteristics at the same positions (upper, middle, and lower parts) of the cladding layers of the specimens are compared and analyzed. Third, the multifunctional composite mechanical test equipment is used to test the tensile properties of the specimens at different laser powers. The stress-strain curve of each specimen is obtained through the test, and then the yield strength, tensile strength, elongation, Young's modulus, and other mechanical property indexes of the respective specimen are calculated. Finally, the macroscopic fracture characteristics of each tensile specimen are observed by scanning electron microscopy (SEM) combined with the stress-strain curves to determine the fracture mode and plasticity of the cladding coating, which can be used to explain the mechanical properties of the specimens at different power levels.

Results and Discussions The experimental analysis shows that with the increase of laser power, the width of the cladding layer gradually increases, and the depth of the heat-affected zone first decreases and then increases (Fig. 4). In the microstructure of the middle of the cladding layer, the organization of the specimen by 1800 W is mainly composed of cellular crystals, and a small number of columnar crystals and dendrites. The organization tends to be uniform, while the morphological organizations of specimens generated at powers of 1500 W, 2100 W and 2400 W are dominated by elongated columnar crystals and larger dendrites (Fig. 5). The plasticity of the cladded specimen increases continuously when the laser power increases from 1500 W to 1800 W. When the laser power increases from 1800 W to 2400 W, the plasticity of the cladded specimen continues to decrease. It can be seen that the mechanical properties of the cladded specimens with a power of 1800 W are the best in all cladded specimens, and the yield strength, tensile strength, Young's modulus, and elongation of these specimens are 655 MPa, 690 MPa, 130 GPa, and 5.3% respectively at this time (Fig. 8). Tiny ligamentous fossae are found in the fractures of the cladding layer (CL), heat-affected zone (HAZ) and substrate, so the specimens generated at 1800 W exhibit the ductile fracture characteristics. In contrast, the specimens generated at powers of 1500 W, 2100 W and 2400 W mainly show the brittle fracture characteristics, and the cleavage steps or river-like brittle cleavage fractures are clearly visible in the cladding layer, the heat affected zone, and the substrate (Fig. 10).

Conclusions The study on the effect of laser power on the mechanical properties of laser cladded 27SiMn steels can be concluded that 1800 W is the optimum power for laser cladding. A laser cladded coating with good mechanical properties is obtained with a laser power of 1800 W, a scanning speed of 20 mm/s, a powder feeding rate of 18 g/min, a defocusing distance of 0 mm, and a spot diameter of 2 mm. The microstructure in the middle of the laser cladded layer of the specimen at 1800 W shows more cytosine crystals and a small number of dendrites and columnar crystals. The more cellular crystals can make the specimen less prone to fracture. The heat-affected zone of the laser cladded coating is the smallest, therefore the damage to the substrate is the lowest and the fracture of the tensile specimen is mainly ductile. Above all, the research results here can provide a good reference for the hydraulic support remanufacturing engineering practice.

Key words laser technique; laser power; microstructure; tensile performance; fracture morphology